energies

MDPI

Article

Research on Capacity Allocation Optimization of Commercial Virtual Power Plant (CVPP)

Songkai Wang [1,2,*], Rong Jia [2,3], Xiaoyu Shi [3,*], Chang Luo [4], Yuan An [3], Qiang Huang [1], Pengcheng Guo [1], Xueyan Wang [3] and Xuewen Lei [1]

[1] School of Water Resources and Hydropower, Xi'an University of Technology, Xi'an 710048, China; sy-sj@xaut.edu.cn (Q.H.); guoyicheng@xaut.edu.cn (P.G.); leixuewen456@163.com (X.L.)
[2] Key Laboratory of Smart Energy in Xi'an, Xi'an University of Technology, Xi'an 710048, China; jiarong@xaut.edu.cn
[3] School of Electrical Engineering, Xi'an University of Technology, Xi'an 710048, China; anyuan@xaut.edu.cn (Y.A.); wxy000113@163.com (X.W.)
[4] Hanjiang-to-Weihe River Valley Water Diversion Project Construction Co., Ltd., Xi'an 710048, China; luochang@hwrvwd.cn
* Correspondence: 1170413040@stu.xaut.edu.cn (S.W.); b21016@xaut.edu.cn (X.S.)

Abstract: Commercial virtual power plants (CVPP) connect the form of renewable energy resource portfolio to the power market and reduce the risk of the unstable operation of a single renewable energy. Combining different kinds of large-scale renewable energy in CVPP to provide capacity services like base load, peak shaving, and valley-filling, etc., for the system loads is an urgent problem to be solved. Therefore, it is valuable to analyze the capacity allocation ratio of the CVPP to maximize the utilization of all kinds of energy, especially for the large-scale multi-energy base. This paper proposed a multi-energy coordinated operation framework by considering various load demands, including base load and peak shaving for the capacity allocation of CVPP based on the world's largest renewable energy resource base on the upstream area of the Yellow River. The main procedures of this framework are as follows: (1) A paratactic model satisfying base load and peak shaving is proposed to determine the ability of the CVPP operation model's capacity services to meet the different demands of the power system load. (2) A hybrid dimension reduction algorithm with a better convergence rate and optimization effect solves the proposed paratactic model based on the ReliefF and the Adaptive Particle Swarm Optimization (APSO). The results show that the large-scale CVPP with different compositions can achieve both of the goals of a stable base load output and stable residual load under different weather conditions. Compared with the operation on sunny days, the base load fluctuation and residual load fluctuation of CVPP on rainy days are reduced by 14.5% and 21.9%, respectively, proving that CVPP can alleviate renewable energy's dependence on weather and improve energy utilization.

Keywords: commercial virtual power plants; capacity allocation; base load; peak shaving; hybrid dimension reduction algorithm

Citation: Wang, S.; Jia, R.; Shi, X.; Luo, C.; An, Y.; Huang, Q.; Guo, P.; Wang, X.; Lei, X. Research on Capacity Allocation Optimization of Commercial Virtual Power Plant (CVPP). *Energies* **2022**, *15*, 1303. https://doi.org/10.3390/en15041303

Academic Editors: Michele Pinelli, Alessio Suman and Nicola Casari

Received: 6 January 2022
Accepted: 22 January 2022
Published: 11 February 2022

1. Introduction

With the continuous increasing proportion of the renewable energy (RER) in the power grid, scholars around the world have proposed virtual power plant (VPP) technology in recent years to realize the integration and control of this RER [1]. Through advanced communication technology and software management systems, VPPs can be considered as the aggregation and optimization of RER, energy storage facilities, controllable loads, and other types of power resources in the power grid [2,3]. VPPs can participate in the power grid operators to coordinate the contradiction between the power grid and RER and realize the optimal allocation and efficient utilization of resources. According to the different functions of VPPs, the EU Fenix project divides VPPs into two categories [4]. One is

technical virtual power plants (TVPP), which provides the system operation, management, balance, and auxiliary services for distribution and transmission system operators on the technical management level [5]. The other is commercial virtual power plants (CVPP), which refers to the virtual power plant from commercial revenue and connects renewable energy resources as a portfolio to the power market [6]. The investment portfolio between renewable energy resources provides diversified energy for the power market and reduces the risk of unbalanced operation of single renewable energy of the power market. Arranging the capacity of various renewable energies in the most appropriate proportion to meet the different needs of the market has become a new problem. Allocating the capacity of renewable energy in CVPP to meet different load requirements and giving full play to the benefits of renewable energy will be the main problem of VPP dispatching operation. Therefore, it is valuable to analyze the capacity allocation ratio of the CVPP to maximize the utilization of all kinds of energy, especially for the large-scale multi-energy base.

Countries worldwide have launched research on the capacity allocation of CVPP. Reference [7] discussed the best capacity of the VPP with wind power and pumped-hydro by considering both the maximum benefit and maximum renewable energy ratio. However, the type of energy is too singular. Reference [8] investigated a unit optimal commitment method by considering the electricity price for a VPP to participate in the electricity market. Reference [9] took the maximum economic benefit of the dispatching model as the objective function. A VPP including thermal power, wind power, CHPS, and pumped storage is constructed. However, photovoltaic was not discussed. Reference [10] proposed a new multi-objective genetic algorithm to evaluate the VPP's capacity proportioning by aiming at the lowest cost. However, the load side demand was not considered. Reference [11] considered the spare capacity and carbon emission cost to propose an improved heuristic method for the capacity planning of the VPP. Reference [12] proposed a VPP project framework by considering the societal benefits and the market proceeds, aiming at cost, revenue, and environmental emission. Reference [13] established a microgrid-type VPP structure and proposed a capacity proportioning model with a game-theory algorithm. However, the scale of the VPP was small. Reference [14] developed a new microgrid two-layer game model by a collaborative subsequence game of different energies to obtain the optimal capacity of a VPP. Reference [15] proposed random scene creation and robust majorization to reduce uncertainty and optimize the VPP capacity proportioning program. Reference [16] configured the capacities of wind/solar/gas microgrids, aiming at providing demand-side services, dealing with emergencies, and supporting system toughness. However, hydropower was not discussed. Reference [17] proposed an island-type VPP capacity proportioning optimization model in view of measuring the cost of renewable power generation. However, this lacked application to large-scale energy scenes. Reference [18] established an optimal model of the electricity and gas combination VPP to obtain optimal operation time and capacity of different energy sources. Reference [19] proposed a new intelligent algorithm that combined the GA and the water drop algorithm to obtain the position and capacity of distributed generation in the microgrid-type VPP. However, the proposed algorithm is too complex. Reference [20] established a mathematical model by using the AHP to analyze the multi-energy capacity ratio and economy. Reference [21] emulated a typical combined cycle power generation unit to analyze the susceptibility of carbon emission and electricity price. Reference [22] considered energy cooperation among different regions to build a multi-energy VPP capacity ratio model, and minimizing the system cost, by proposing a random scene creation. However, the impact of the load side was not discussed. Reference [23] proposed a two-layer model for the full life cycle of the muti-energy system to obtain the minimum economic cost and the optimal control strategy.

The past studies have many common deficiencies on the capacity allocation of CVPP: (1) Capacity allocation research is usually from the perspective of power generation. The built model aims to minimize power generation cost or maximize economic benefit [24], which does not consider the load demand, and the operating mode is too singular. (2) The capacity allocation studies of VPPs are mainly for the small capacity systems, microgrids,

and Combined Cooling Heating and Power (CCHP) [25,26]. Only a few studies have been conducted on sizeable virtual power plants with large-scale renewable energy. (3) The previous research always chose typical GA, PSO, DE, and other algorithms to solve the model [27,28], which could easily fall into a local convergence and gain inaccurate results.

In order to supplement and innovate the previous research, this paper provides a new study framework for the capacity allocation of CVPP by considering different load demands. The main contributions are as follows: (1) A paratactic model combining the base load type (BLT), which is responsible for the stable part of the power system load, and the peak shaving type (PST), which is responsible for the peak part of the power system load, is proposed for determining the operation model of CVPP. (2) A hybrid dimension reduction algorithm on ReliefF and APSO is a new avenue for resolving the proposed paratactic model. The built framing is tested by the world's largest renewable energy resource base on the upstream area of the Yellow River.

The research structure of this paper is as follows: the CVPP's capacity allocation modeling and the hybrid dimension reduction algorithm based on ReliefF and APSO are described in Section 2. Section 3 probes into a case study, and Section 4 examines its results. Finally, the conclusions of the study are drawn in Section 5.

2. Method

By uniting the CVPP generation power curve and the load curve, this paper divides the CVPP capacity allocation model into the base load type (BLT), which is responsible for the stable part of power system load, and the peak shaving type (PST), which is responsible for the peak part of the power system load. A hybrid dimension reduction algorithm on ReliefF and APSO is a new avenue for resolving the paratactic model. The flowchart of the proposed the CVPP capacity allocation framework is shown in Figure 1.

2.1. CVPP Capacity Allocation Modeling

2.1.1. Base Load Type

The base load type is responsible for the stable part of the power system load to operate under high-efficiency conditions as far as possible. The model is used to discuss the practicability of CVPP and compute the most steady capacity allocation.

The base load type CVPP analyzed in this section includes wind power, photovoltaic, and hydropower. Aiming at the minimum fluctuation of CVPP output, the model calculates various energy capacity allocations as follows

$$\min F_1 = \sqrt{\frac{1}{T-1}\sum_{t=1}^{T}(P_t - P(av))} \quad (1)$$

$$P_t = \alpha P_p(t) + (1-\alpha)\beta P_w(t) + (1-\alpha)(1-\beta)P_h(t) \quad (2)$$

where F_1 denotes the standard deviation of P_t; P_t denotes the total out power of CVPP, the F_1 value and the total output fluctuation are in the direct ratio; $P_p(t)$, $P_w(t)$, and $P_h(t)$ denote the photovoltaic power, wind power, and hydropower generation, respectively, the calculation formulas will be introduced in Section 2.2; α and β denote the weight—α is the proportion of photovoltaic power in total CVPP output, $(1-\alpha)\beta$ is the wind power proportion in total CVPP output, $(1-\alpha)(1-\beta)$ is the hydropower proportion in total CVPP output. Then, when $\alpha = 1$, it is combined into 100% photovoltaic; when $\alpha = 0$ and $\beta = 1$, means 100% wind power generation; when $\alpha = 0$ and $\beta = 0$, means 100% hydropower generation.

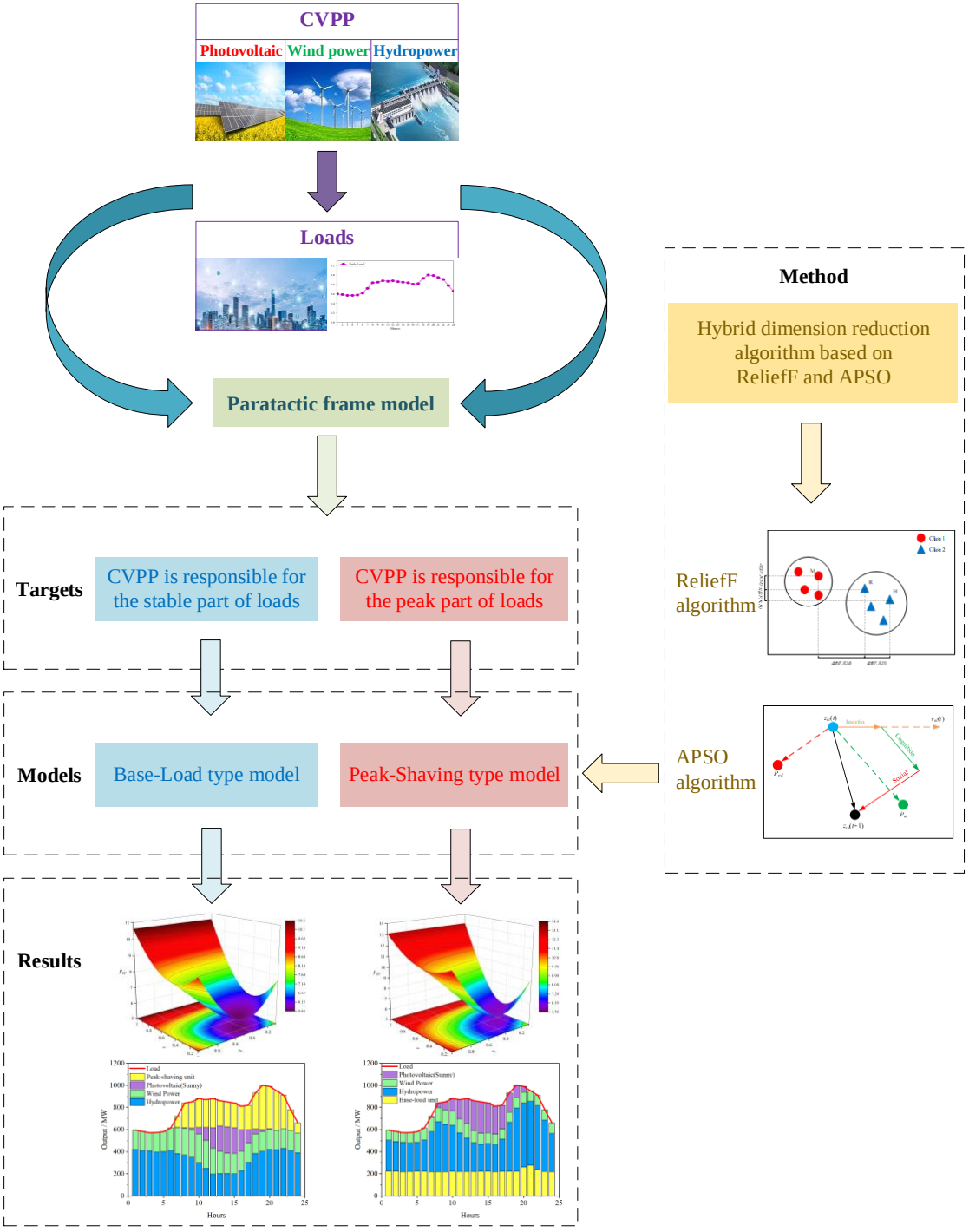

Figure 1. The flowchart of the proposed CVPP capacity allocation framework.

2.1.2. Peak Shaving Type

The peak shaving type is responsible for the peak part of the power system load, making the residual load allocated to power sources with poor regulation capacity such as thermal power more stable. The peak shaving type will reduce the number of startups and shutdowns of thermal power units, save startup consumption, improve the overall operational efficiency of the power station.

The peak shaving type aims at minimizing the mean square deviation of residual load after deducting wind power, photovoltaic, and hydropower in CVPP from grid load [29]. The formula is as follows

$$\min F_2 = \sqrt{\frac{1}{T}\sum_{t=1}^{T}[R_t - \frac{1}{T}\sum_{t=1}^{T}R_t]^2} \tag{3}$$

$$R_t = L_t - \alpha P_P(t) - (1-\alpha)\beta P_W(t) - (1-\alpha)(1-\beta)P_H(t) \tag{4}$$

where F_2 denotes the mean square deviation of R_t; R_t denotes the residual load after deducting wind power, photovoltaic, and hydropower, the larger the F_2 value, the greater the residual load fluctuation, and the smaller the F_2 value, the smaller the residual load fluctuation; $P_p(t)$, $P_w(t)$, and $P_h(t)$ denote the photovoltaic power, wind power, and hydropower generation, respectively; the remaining variables are the same as shown in Section 2.1.1.

2.2. Power Modeling

The CVPP in this paper only includes photovoltaic, wind, and hydropower.

(1) Wind power model

The wind power output P_w is the power generation of wind turbines under different wind speed conditions, and will be calculated as follows [30]

$$P_w = \begin{cases} 0 & v \le v_i \quad or \quad v \ge v_o \\ P_r \frac{v - v_i}{v_r - v_i} & v_i \le v \le v_r \\ P_r & v_r \le v \le v_o \end{cases} \tag{5}$$

where P_r denotes the rated wind output under the rated conditions; v denotes the real-time wind speed; v_i denotes the cut-in wind speed; v_o denotes the cut-out wind speed; v_r denotes the rated wind speed.

(2) Photovoltaic model

The photovoltaic output P_p is linearly related to the solar light intensity, and is calculated as follows [31]

$$P_p = P_r \frac{G}{G_r}[1 + \alpha_T(T - T_r)] \tag{6}$$

where P_r denotes the rated photovoltaic output under the rated conditions; G denotes the actual solar irradiance (W/m^2); G_r denotes the rated solar irradiance (1000 W/m^2); a_T denotes the temperature coefficient; T denotes the actual surface temperature of the photovoltaic cells (°C); T_r denotes the rated surface temperature of the photovoltaic cells (25 °C) [32].

(3) Hydropower model

This study only deals with reservoir power plants. The high water period, low water period, environmental flows (such as meltwater, rainfall, evaporated water, etc.), and tributary flows are all not considered for simplifying the calculation in this study. The output power P_h will be calculated as follows [33]

$$P_h = \eta_h g h \rho Q \tag{7}$$

where g denotes the gravitational acceleration (9.81 m/s^2); η_h denotes the efficiency of the generator; ρ denotes the density of the water (1000 kg/m^3); Q denotes the water flow (m^3/s); h denotes the height of the water drop (m).

The constraints of wind power, photovoltaic, and hydropower are as follows [34]

$$0 \le P_W \le P_{W,\max} \tag{8}$$

$P_{W,max}$ denotes the wind power rated output (MW);

$$0 \le P_P \le P_{P,\max} \tag{9}$$

$P_{P,max}$ denotes the photovoltaic rated output (MW);

$$V_{t+1} = V_t + (I_t - Q_t)\Delta t \tag{10}$$

V_{t+1} and V_t denotes the reservoir storage (m^3) at the end and the beginning, respectively; I_t denotes the reservoir inflow (m^3/s);

$$V_t^l \le V_t \le V_t^u \tag{11}$$

$V_t{}^l$ and $V_t{}^u$ denote the lower and upper limits for reservoir storage (m^3), respectively;

$$Q_{t\min} \le Q_t \le Q_{t\max} \tag{12}$$

$Q_t{}^l$ and $Q_t{}^u$ denote the lower and upper limits for river discharge flow (m^3/s), respectively;

$$N_t^l \le N_t \le N_t^u \tag{13}$$

$N_t{}^l$ denotes the lower limits for hydropower output (MW) (The output of the reservoir must be discharged for meeting the downstream irrigation, water supply, navigation, etc.); $N_t{}^u$ denotes the upper limits for hydropower output (MW);

$$N_s = N_t - N_t^l \tag{14}$$

N_s denotes the schedulable output (MW), which refers to the output that the hydropower can offer in CVPP on the satisfying water dispatching premise.

2.3. Hybrid Algorithm Based on ReliefF and APSO

2.3.1. APSO Algorithm

Virtual power plant optimal scheduling is a typical power system optimization problem with high dimension, nonlinearity, and multi-constrained. Compared with genetic algorithms and other algorithms, the PSO algorithm is a better algorithm for optimizing and solving the problem.

Each particle in the PSO algorithm is described by position and velocity vectors [35]. Assuming the total number of particles is M, the position and velocity of the nth particle in dimension d are as follows

$$\begin{cases} X'_n = (x'_{n1}, x'_{n2}, ..., x'_{nd})^T, n = 1, 2, ..., M \\ V'_n = (v'_{n1}, v'_{n2}, ..., v'_{nd})^T, n = 1, 2, ..., M \end{cases} \tag{15}$$

Each particle adjusts its speed and position by tracing the last best individual position and best group position, which are expressed as follows

$$\begin{cases} P'_n = (P'_{n,1}, P'_{n,2}, ..., P'_{n,d}) \\ P'_g = (P'_{g,1}, P'_{g,2}, ..., P'_{g,d}) \end{cases} \tag{16}$$

where P_n denotes the individual optimal position of the nth particle; P_g denotes the best position of the group obtained from all particles in the previous iteration.

The speed and position update formula of the PSO algorithm is presented as follows

$$\begin{cases} X_{nd}^{k+1} = X_{nd}^k + V_{nd}^{k+1} \\ V_{nd}^{k+1} = \omega' V_{nd}^k + c'_1 r'_1 (P_{nd}^k - X_{nd}^k) + c'_2 r'_2 (P_{gd}^k - X_{nd}^k) \end{cases} \tag{17}$$

where ω denotes the inertia weight factor. c_1' and c_2' denote the learning factor; r_1' and r_2' denote the uniformly distributed random numbers (0, 1).

The PSO algorithm often has premature convergence and other problems in dealing with multi-extreme function problems. The Adaptive Particle Swarm Optimization (APSO) algorithm is adopted by adding inertial frames during speed update to help particles quit of local extreme values [36]. The formula is as follows

$$\omega' = (\omega'_{max} - \omega'_{min}) \times \exp(-(\tau \times \frac{k}{K_{max}})^2) + \omega'_{min} \quad (18)$$

where ω'_{max} and ω'_{min} denote the maximum and minimum inertia coefficients; K_{max} denotes the maximum Iterations; τ denotes the empirical value, generally within (20, 55). Larger ω' makes APSO have strong whole region searchability, while smaller ω' tends to local search. The APSO can achieve different search results by changing the inertia coefficient. With the gradual reduction in inertia coefficient, the algorithm also has the initial global search to the later local search.

2.3.2. ReliefF Algorithm

Although the APSO algorithm can solve the traditional PSO algorithm's problems, it is easy to fall into local optimization and premature convergence to a certain extent. Sometimes, a single algorithm cannot obtain the optimization results because of its defects. For example, the APSO algorithm has strong global searchability and weak local searchability in the initial stage, which will result in low computational efficiency in the initial step of the CVPP optimal scheduling model. Therefore, selecting an appropriate algorithm to supplement this shortcoming is the focus of this paper.

Feature selection is a prevalent dimensionality reduction method with solid local searchability. It refers to selecting the feature subset that makes a certain evaluation standard optimal from the original feature set. Its purpose is to select some of the most valuable features to reduce the data feature dimension and make the chosen optimal feature subset approximate or even better prediction results before feature selection. It improves the generalization ability and the calculation efficiency of the model, the data's actual utility, and reduces the frequency of dimensional disasters.

The core content of the ReliefF algorithm is the correlation between features and dataset class marks [37]. ReliefF algorithm randomly selects a sample R from the training set. Find k samples that belong to the same class as R and are closest to it, which is called *NearHit*, and then find k samples that belong to a different class from R and are closest to it, which is called *NearMiss*. The weight is obtained according to the following algorithm:

(1) Calculate ${S_A}^{Hit}$, the distance between R and *NearHit* on each feature A.
(2) Calculate ${S_A}^{Miss}$, the distance between R and *NearMiss* on each feature A.
(3) Compare the two distances ${S_A}^{Hit}$ and ${S_A}^{Miss}$. If ${S_A}^{Hit}$ is greater than ${S_A}^{Miss}$, each feature of the A is helpful to distinguish the same kind and different kinds. If ${S_A}^{Hit}$ is less than ${S_A}^{Miss}$, each feature of the A hurts, distinguishing the same class and different classes and reduces the weight of the feature.
(4) Repeat the above process m times to gain the average weight of each feature, as is shown in Formula (19)

$$W(A) = -\sum_{j=1}^{k} diff(A, R, H_j)/mk + \sum_{C \notin class(R)} [\frac{p(C)}{1 - p(class(R))} \sum_{j=1}^{k} diff(A, R, M_j(C))]/mk \quad (19)$$

where *diff*(A,R,H_j) denotes the difference between sample R and H_j in feature A, as is shown in Formula (20); $M_j(C)$ denotes the *j-th* nearest sample in category C; $p(C)$ denotes

the target probability of class C, given by Formula (21). When the number of samples is approximately the same, there are $p(C) = 1/C$.

$$diff(A, R_1, R_2) = \frac{|R_1[A] - R_2[A]|}{\max(A) - \min(A)} \tag{20}$$

$$p(C) = \frac{N_c}{\sum_{c=1}^{C} N_c} \tag{21}$$

After m repetitions, each feature gets an average weight. The larger the average weight, the better the feature is at distinguishing different categories. The smaller the average weight, the worse the feature is at distinguishing different categories.

2.3.3. ReliefF–APSO Hybrid Algorithm

This paper combines the ReliefF with the APSO to obtain a better hybrid algorithm by using the advantages of the ReliefF algorithm's strong local searchability and the APSO algorithm's strong global optimization ability. The ReliefF–APSO hybrid algorithm can make the particle positions in a sub-population relatively concentrated and learning relatively easy, and improve the search efficiency, spending limited time on the most effective search. The structure diagram of the ReliefF–APSO hybrid algorithm is shown in Figure 2.

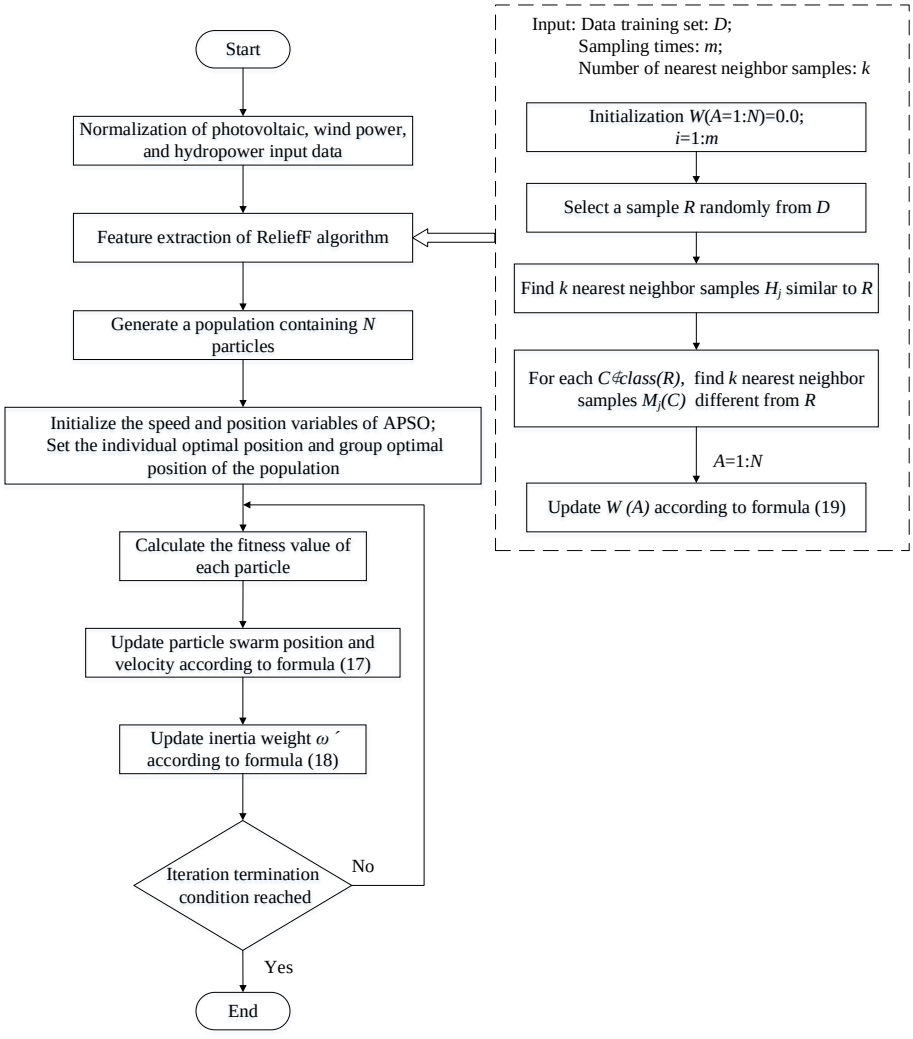

Figure 2. Flowchart for the ReliefF–APSO hybrid algorithm.

The steps of the hybrid algorithm are as follows:

(1) The given data set is normalized by Z-score before training;
(2) Using the Formula (19) to extract the features of the ReliefF algorithm and take the first d features with relatively large weight as the training set and test set of APSO, $d = 100$;
(3) Generate population, set the number of particles N, set each particle as a random number vector within $(-1, 1)$, and set the number of neurons and hidden layer nodes. In the experiment, N takes 20;
(4) Initialize the speed and position variables of APSO, and set the individual optimal position and group optimal position of the population;
(5) Calculate the fitness value of each particle;
(6) Update the position and velocity of the adaptive particle swarm according to Formulas (17) and (18);
(7) Judge whether the maximum number of iterations is reached. If so, stop the iteration. Otherwise, turn to step (5) and continue the iteration.

3. Case Study

The built framing is tested using the world's largest renewable energy resource base on the upstream area of the Yellow River in China. This area is in the southeast of Qinghai Province, China, and is rich in photovoltaic, wind power, hydropower, and other renewable energy resources [38]. The location of the upstream area of the Yellow River is shown in Figure 3.

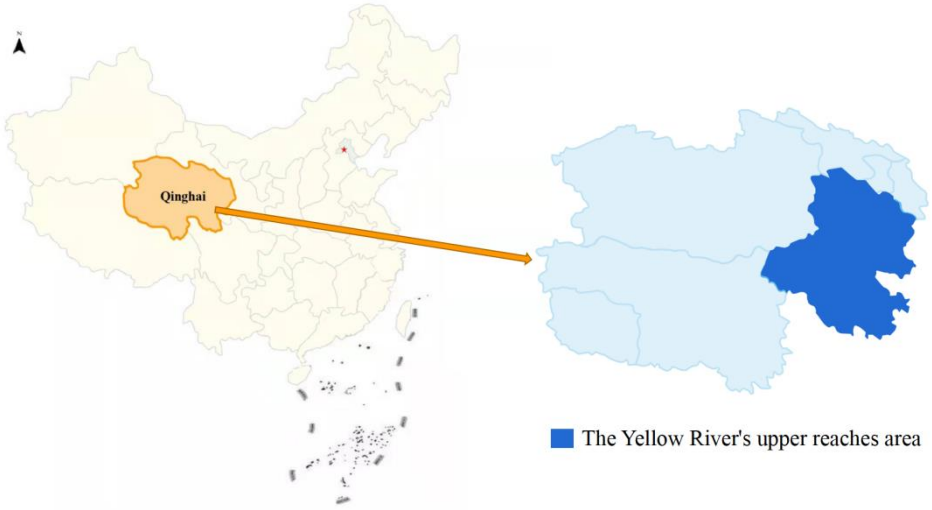

Figure 3. Location of the upstream area of the Yellow River.

The data of wind speed, wind force, temperature, and solar radiation of Gonghe observation point and Xinghai observation point in the upstream area of the Yellow River are provided by the China Integrated Meteorological Information Sharing System (CIMISS). The mean daily wind speed and daily maximum total irradiance in 2019 are shown in Figure 4. The Yellow River's historical hydrological data provides hydropower output.

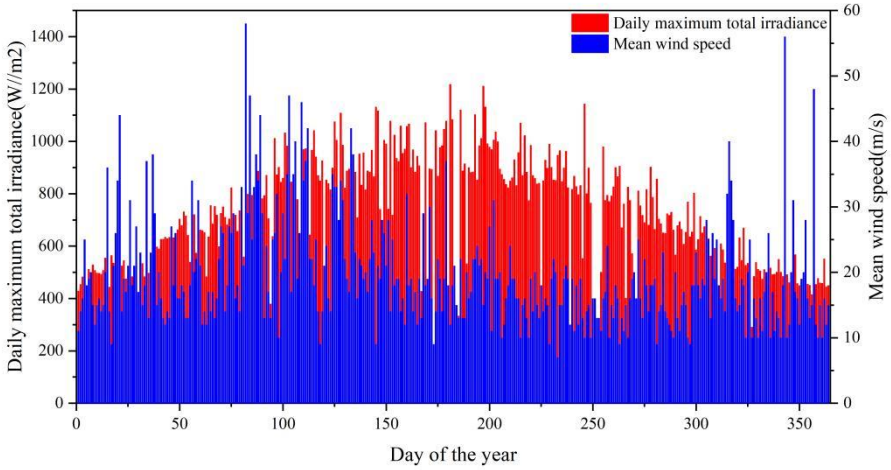

Figure 4. Data map for wind and solar resources of the upstream area of the Yellow River.

4. Results and Discussion

Due to the instability of renewable energy output, it can only participate in the medium- or long-term power market, which cannot be a member of the spot market that needs flexible adjustment [39]. The integration of renewable energy through CVPP can improve the stability and flexibility of the system and enable renewable energy to participate more in the day-ahead and real-time market. This paper selects the daily scale as the research scope, and the typical daily load curve data and typical daily renewable energy output data including sunny and rainy days, are selected to avoid the impact of renewable energy and load uncertainty. The typical daily hourly output of renewable energies and the daily hourly load curve of the target area in the study area are shown in Figure 5.

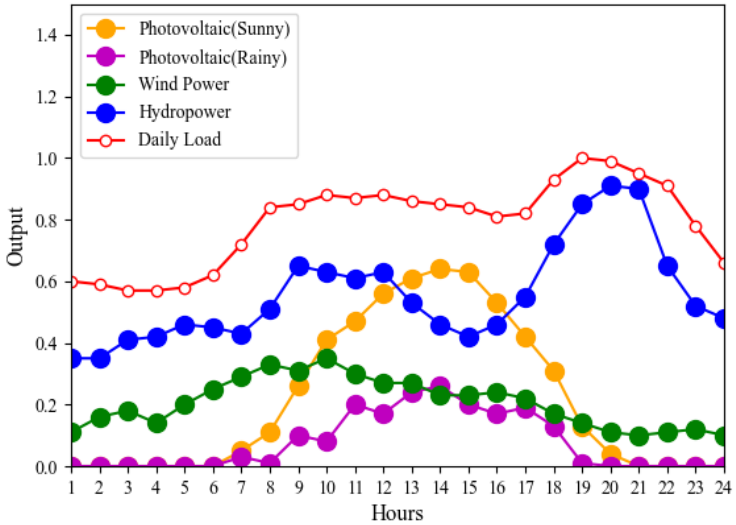

Figure 5. The hourly output and daily load curve.

Using Python3.7 to simulate the proposed paratactic model. This section sets the total installed capacity of CVPP to be 1000 MW. This chapter assumes that at the beginning of the calculation, each kind of energy has the same capacity proportion and contribution to the CVPP. The value range of weight α and β from Equations (2) and (4) is (0, 1), and the change step is 0.01.

4.1. Comparative Analysis of ReliefF–APSO Hybrid Algorithm, APSO, and PSO

The ReliefF–APSO hybrid algorithm, APSO, and PSO are respectively used for solving the base load type operation model on sunny days. In the PSO algorithm, w = 0.6, learning

factor $c_1 = c_2 = 2$. In the ReliefF–APSO hybrid algorithm and APSO algorithm, $w_{max} = 0.9$, $w_{min} = 0.4$, and learning factor $c_{1a} = c_{2a} = 2$. The number of particles is 20 and the maximum number of iterations is 100. The results of the algorithm comparison are shown in Figure 6.

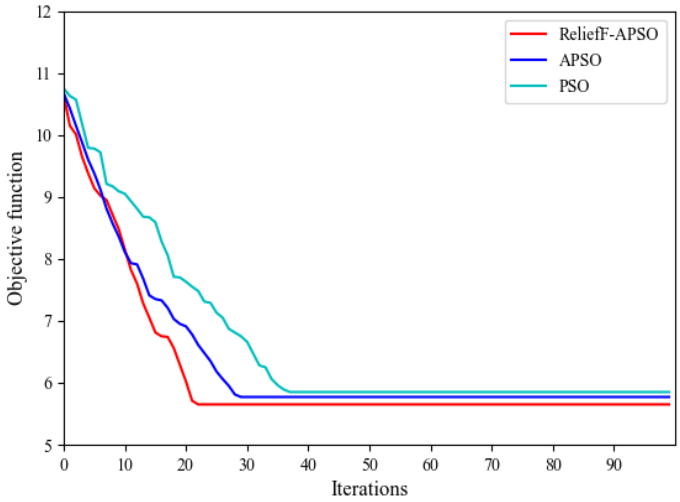

Figure 6. Algorithm comparison between the ReliefF–APSO, APSO, and PSO.

The ReliefF–APSO hybrid algorithm gains the lowest objective function and finds the optimal solution in the 23rd iteration. In contrast, the APSO algorithm finds the optimal solution in the 30th iteration, and the PSO algorithm finds the optimal solution in the 38th iteration. The convergence rate of the ReliefF–APSO hybrid algorithm is 23.33% quicker than the APSO and 39.47% quicker than the PSO. Moreover, the smoothness of the curve shows that the optimization effect of the ReliefF–APSO hybrid algorithm is better than that of the APSO and PSO.

4.2. Base load Type Operation Model

The base load type is responsible for the relatively stable "basic" part of the load, which takes the minimum fluctuation of the total output power of CVPP as the optimization goal. Peak shaving is distributed to thermal power and other energy. The results of the energy proportion of the base load type operation on sunny and rainy days are shown in Figure 7.

When the output of CVPP is all composed of photovoltaic output, the total output fluctuates the most because compared with wind power and hydropower, photovoltaic fluctuates the most in a day. When the output composition of CVPP is 25% photovoltaic, 27% wind power, and 48% hydropower, the fluctuation of total output on sunny days is the smallest. The small proportion of photovoltaic is because photovoltaic can only provide daytime output, but its fluctuation is too strong to maintain the stability of total output. Wind power has output all day, so the proportion is slightly higher than that of photovoltaic.

When the output composition of CVPP is 4% photovoltaic, 18% wind power, and 78% hydropower, the total output fluctuation on rainy days is the smallest. On rainy days, the system's total output needs to be mainly borne by hydropower with stronger regulation capacity because the PV output is too small, and the wind power output fluctuates strongly.

The smallest F_1 is 5.65 on sunny days and 4.83 on rainy days, which means the CVPP output on rainy days is more stable. That is because on rainy days, the proportion of photovoltaic is small, and the proportion of hydropower is high, which is more conducive to maintaining the stability of the overall output. The largest F_1 is 10.63 on sunny days and 13.09 on rainy days, which means compared to the single energy mode, the CVPP could reduce the base load fluctuation by 46.8% on sunny days and 63.1% on rainy days. The operation results of the base load type in different weather are shown in Figure 8.

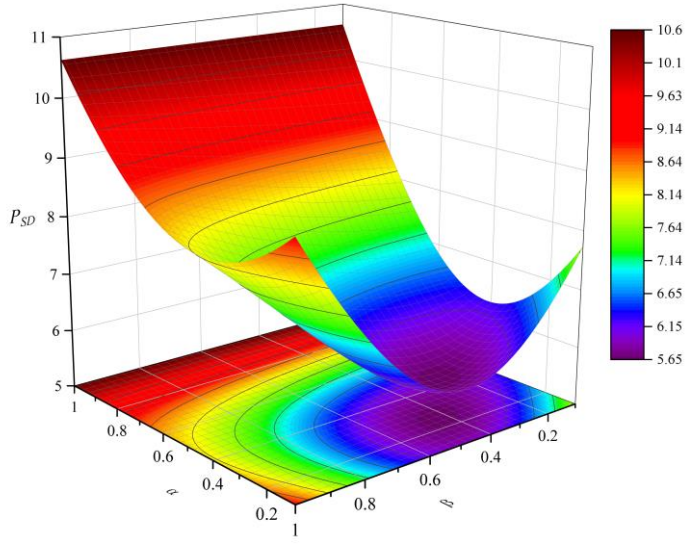

(**a**)

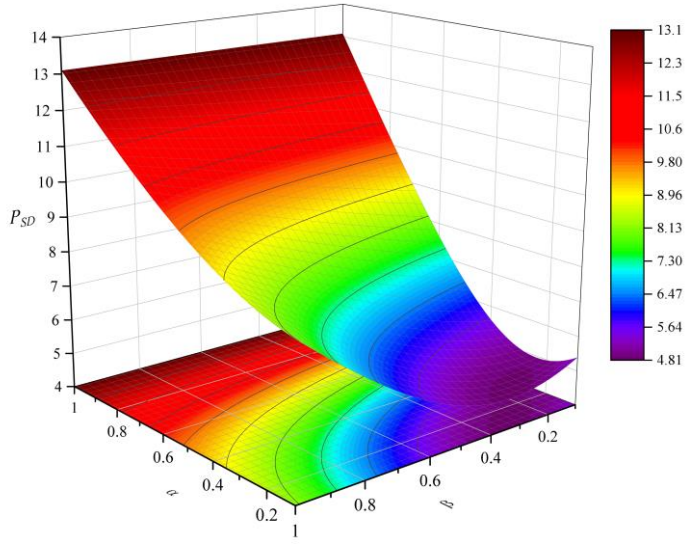

(**b**)

Figure 7. The energy proportion of the base load type operation. (**a**) Sunny days; (**b**) rainy days.

Although the output composition of the base load type CVPP is different on sunny and rainy days, both operation results show that the stability of the base load is well maintained. On sunny days, the output of photovoltaic is remarkable between 9:00 and 19:00, and meets the crest value between 12:00 and 16:00. To ensure photovoltaic consumption and maintain the stability of total output, the hydropower output needs to be reduced during this period. On rainy days, the photovoltaic output is unstable and undulates, which leads to the proportion of photovoltaic being very small. The stability of the base load is mainly guaranteed by hydropower and wind power. As is shown in Figure 9, the results show that the CVPP output fluctuation on rainy days is 14.5% more than on sunny days.

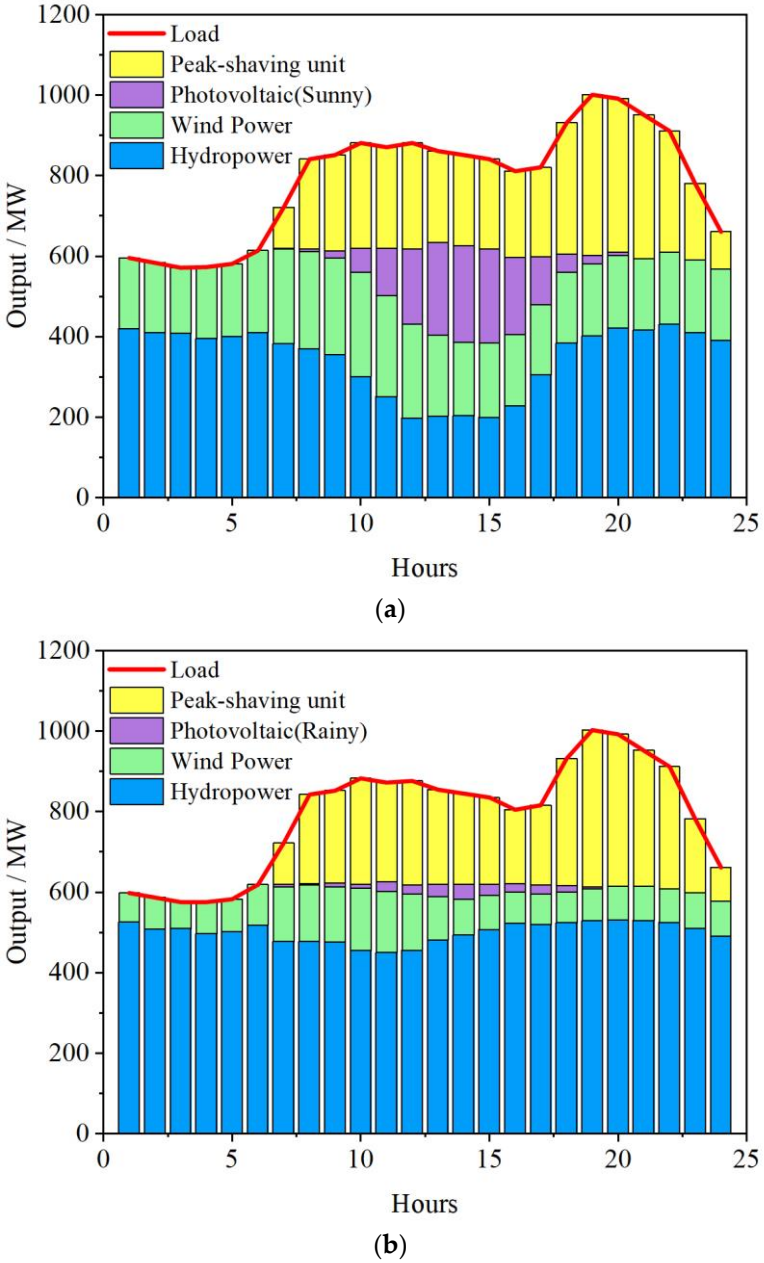

Figure 8. The operation results of the base load type. (**a**) Sunny days; (**b**) rainy days.

4.3. Peak shaving Type Operation Model

The peak shaving type takes the minimum mean square deviation of the residual load after deducting wind power, photovoltaic, and hydropower from the grid load as the optimization goal. It makes the residual load distributed to the power supply with poor regulation capacity more stable, such as thermal power. The results of the energy proportion of the peak shaving type operation on sunny and rainy days are presented in Figure 10.

When the output composition of CVPP is 29% photovoltaic, 13% wind power, and 58% hydropower, the residual load fluctuation is the smallest. The higher proportion of PV is due to the high photovoltaic output on sunny days, which can participate more in peak shaving in the early peak hours to reduce the demand for residual load at peak hours and stabilize thermal power output.

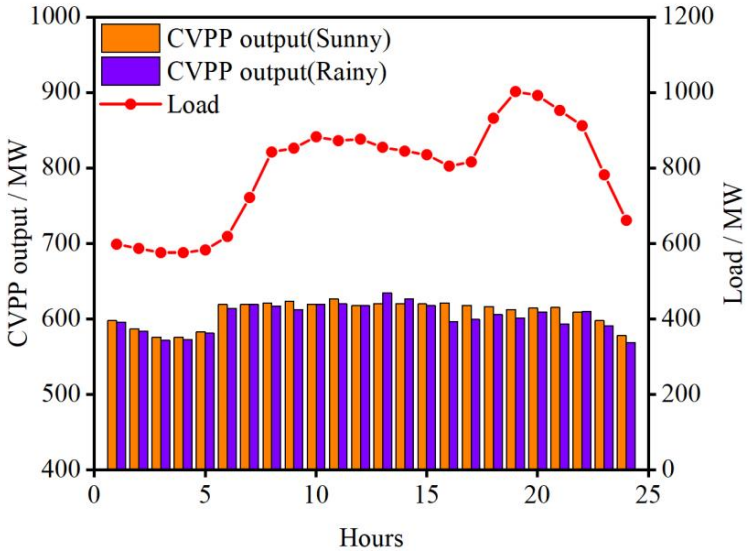

Figure 9. The CVPPV output of the base load type.

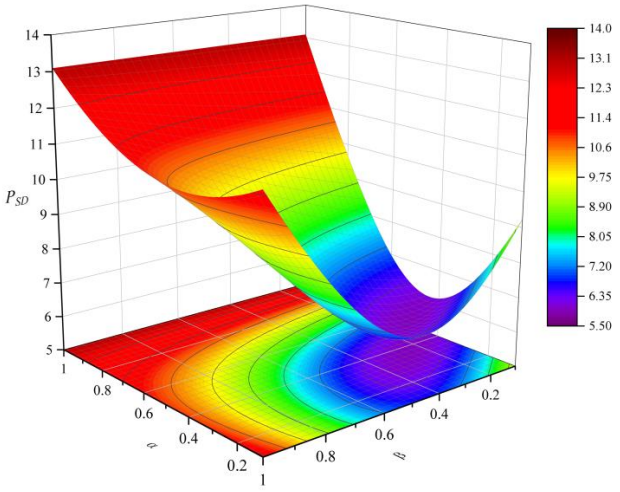

(**a**)

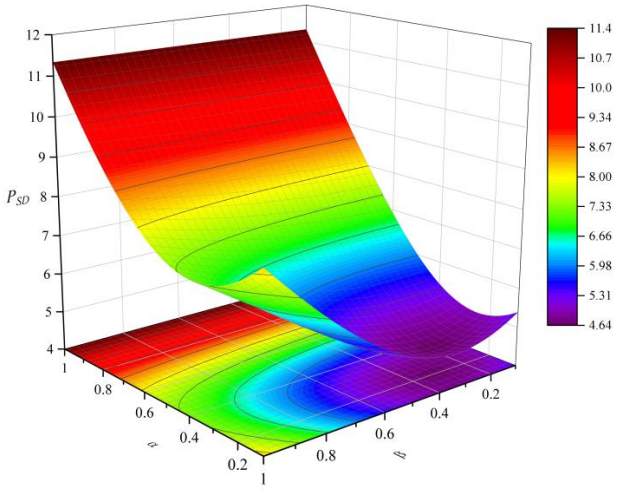

(**b**)

Figure 10. The energy proportion of the peak shaving type operation. (**a**) Sunny days; (**b**) rainy days.

On rainy days, the hydropower station needs to consider flood control factors and cannot fully participate in peak shaving. Therefore, the proportion of hydropower should not be too high, and wind power and some photovoltaic power are needed to assist peak shaving. When the output composition of the virtual power plant is 12% photovoltaic, 22% wind power, and 66% hydropower, the residual load fluctuation is the smallest, and the system peak shaving is mainly completed by hydropower and wind power. The operation results of the peak shaving type in different weather are shown in Figure 10.

The smallest F_2 on sunny days is larger than on rainy days, which means the residual load on rainy days is more stable than on sunny days. That is because, on sunny days, the proportion of photovoltaic is large. However, it cannot provide the peak shaving power at the evening peak, so more thermal power and other energy are needed to help hydropower and wind power for peak shaving. The largest F_2 is 13.09 on sunny days and 11.34 on rainy days, which means compared to the single energy mode, the CVPP could reduce the residual load fluctuation by 54.3% on sunny days and 58.8% on rainy days. The operation results of the peak shaving type in different weather are shown in Figure 11.

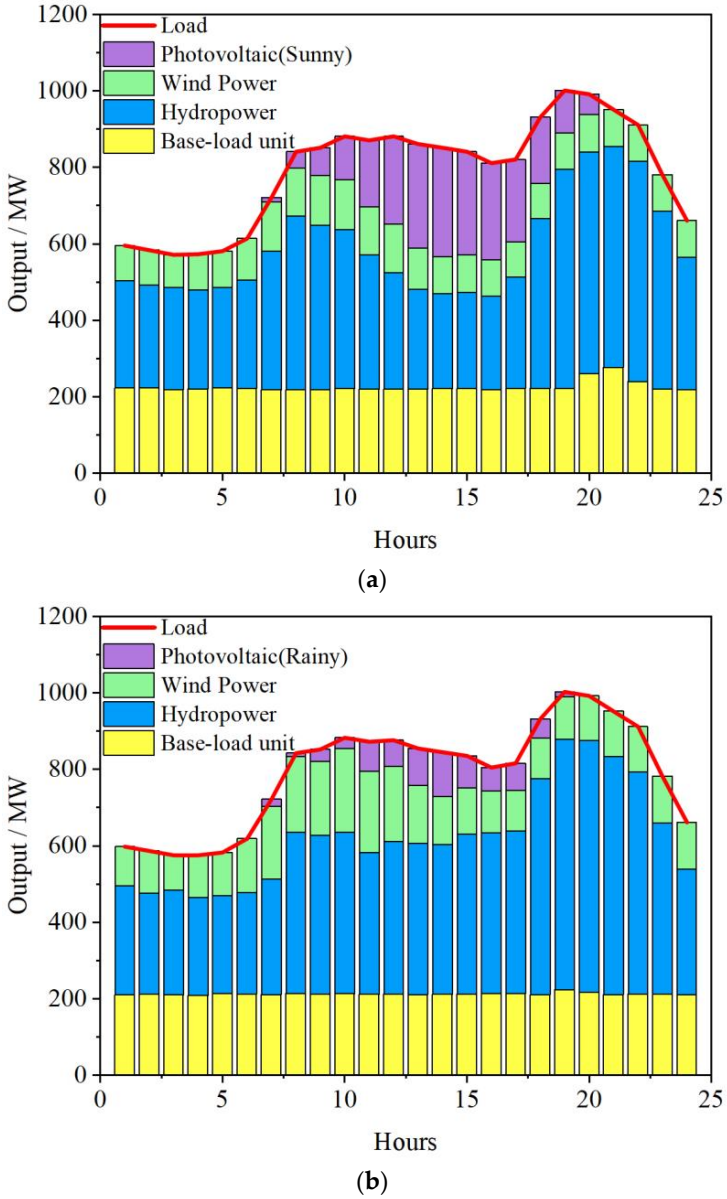

Figure 11. The operation results of the peak shaving type. (**a**) Sunny days; (**b**) rainy days.

Both operation results of sunny days and rainy days show that the residual load of the system has good stability through the CVPP peak shaving. Since the photovoltaic has no output in the evening, the peak shaving assignment is completed by hydropower and wind power during the evening peak period from 19:00 to 22:00. As is shown in Figure 12, on sunny days, photovoltaic has almost no output from 20:00, thus hydropower and wind power cannot satisfy the system peak shaving capacity. Then, the residual load of the system increases, which means that more thermal power and other units partake in the peak shaving. On rainy days, due to the small proportion of photovoltaic and large proportion of hydropower, the peak shaving capacity can be met by the CVPP without additional units. It can be seen that the residual load fluctuation on rainy days is 21.9% more than on sunny days.

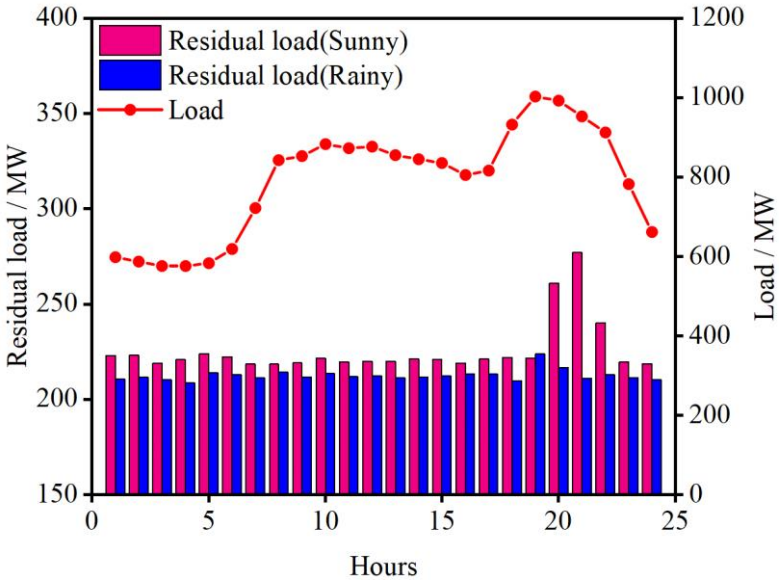

Figure 12. The residual load of the peak shaving type.

The results of this section confirm that the integration of renewable energy through CVPP can provide more stable and flexible power generation resources for system load. Compared to the single energy mode, the CVPP could reduce the base load fluctuation and the residual load fluctuation on both sunny and rainy days, while the base load fluctuation is reduced by 46.8% on sunny days and 63.1% on rainy days, and the residual load fluctuation is reduced by 54.3% on sunny days and 58.8% on rainy days. The base load fluctuation and residual load fluctuation of CVPP on rainy days are reduced by 14.5% and 21.9% more than on sunny days, respectively, proving that CVPP can alleviate renewable energy dependence on weather and improve energy utilization.

5. Conclusions

This paper's research shows that the percentage of CVPP composition is related to the region and available resources. At the same time, large-capacity CVPP can be responsible for different functions of base load and peak shaving in the power market, which can select different renewable energy ratios according to different weather. The convergence rate of the proposed ReliefF–APSO hybrid algorithm is 23.33% quicker than the APSO and 39.47% quicker than the PSO, and the optimization effect of the ReliefF–APSO hybrid algorithm is also better than that of the APSO and PSO. The output compositions of the CVPP on sunny days are 25% photovoltaic, 27% wind power, and 48% hydropower for the base load type, and 39% photovoltaic, 23.2% wind power, and 37.8% hydropower for the peak shaving type. The output compositions of the CVPP on rainy days are 4% photovoltaic, 18% wind power, and 78% hydropower for the base load type, and 12% photovoltaic, 22% wind power, and 66% hydropower for the peak shaving type. The research of this

paper will provide the basis for the flexible capacity allocation construction of CVPP and provide diversity for the selection of VPP services on the user side of the power market.

In practical projects, the services to be provided by CVPP are not limited to base load and peak shaving, and there will be more and more complex working conditions. At the same time, there are many changes in climate and seasons, and the operation of CVPP needs more accurate research.

Author Contributions: For research articles, conceptualization, S.W. and X.S.; methodology, S.W. and R.J.; software, S.W.; validation, C.L., and P.G.; formal analysis, S.W. and X.W.; investigation, S.W. and Y.A.; resources, Q.H. and X.S.; data curation, S.W. and X.L.; writing—original draft preparation, S.W.; writing—review and editing, R.J. and P.G.; visualization, S.W. and C.L.; supervision, R.J.; project administration, R.J. and Y.A.; funding acquisition, R.J. and Q.H. All authors have read and agreed to the published version of the manuscript.

Funding: This work was supported by the National Natural Science Foundation of China (no. 51779206), the Key Projects of Science and Technology Department of Shaanxi Province (2018ZDXM-GY-169), and the Key Industry Innovation Chain Project of Science and Technology Department of Shaanxi Province (2019ZDLGY18-03).

Institutional Review Board Statement: Not applicable.

Informed Consent Statement: Not applicable.

Data Availability Statement: Not applicable.

Conflicts of Interest: The authors declare no conflict of interest.

References

1. Shafiekhani, M.; Ahmadi, A.; Homaee, O.; Shafie-khah, M.; Catalão, J.P. Optimal bidding strategy of a renewable-based virtual power plant including wind and solar units and dispatchable loads. *Energy* **2022**, *239*, 122379. [CrossRef]
2. Rouzbahani, H.M.; Karimipour, H.; Lei, L. A review on virtual power plant for energy management. *Sustain. Energy Technol. Assess.* **2021**, *47*, 101370. [CrossRef]
3. Naval, N.; Yusta, J.M. Virtual power plant models and electricity markets—A review. *Renew. Sustain. Energy Rev.* **2021**, *149*, 111393. [CrossRef]
4. Kieny, C.; Berseneff, B.; Hadjsaid, N.; Besanger, Y.; Maire, J. On the concept and the interest of virtual power plant: Some results from the European project FENIX. In Proceedings of the 2009 IEEE Power & Energy Society General Meeting, Calgary, AB, Canada, 26–30 July 2009; pp. 1–6. [CrossRef]
5. Foroughi, M.; Pasban, A.; Moeini-Aghtaie, M.; Fayaz-Heidari, A. A bi-level model for optimal bidding of a multi-carrier technical virtual power plant in energy markets. *Electr. Power Energy Syst.* **2021**, *125*, 106397. [CrossRef]
6. Elgamal, A.H.; Kocher-Oberlehner, G.; Robu, V.; Andoni, M. Optimization of a multiple-scale renewable energy-based virtual power plant in the UK. *Appl. Energy* **2019**, *256*, 113973. [CrossRef]
7. Papaefthymiou, S.V.; Papathanassiou, S.A. Optimum sizing of wind-pumped-storage hybrid power stations in island systems. *Renew. Energy* **2014**, *64*, 187–196. [CrossRef]
8. Peik-Herfeh, M.; Seifi, H.; Sheikh-El-Eslami, M.K. Decision making of a virtual power plant under uncertainties for bidding in a day-ahead market using point estimate method. *Int. J. Electr. Power Energy Syst.* **2013**, *44*, 88–98. [CrossRef]
9. Pandžić, H.; Kuzle, I.; Capuder, T. Virtual power plant mid-term dispatch optimization. *Appl. Energy* **2013**, *10*, 134–141. [CrossRef]
10. Dufo-López, R.; Bernal-Agustín, J.L.; Yusta-Loyo, J.M.; Domínguez-Navarro, J.A.; Ramírez-Rosado, I.J.; Lujano, J.; Aso, I. Multi-objective optimization minimizing cost and life cycle emissions of stand-alone PV–wind–diesel systems with batteries storage. *Appl. Energy* **2011**, *88*, 4033–4041. [CrossRef]
11. Olamaei, J.; Nazari, M.E.; Bahravar, S. Economic environmental unit commitment for integrated CCHP-thermal-heat only system with considerations for valve-point effect based on a heuristic optimization algorithm. *Energy* **2018**, *159*, 737–750. [CrossRef]
12. Li, J.; Sang, C. Discussion on optimal planning and operation framework for integrated energy system. *Electr. Power Constr.* **2015**, *36*, 41–48. [CrossRef]
13. Shunping, J.; Shoupeng, W.; Fang, F. Game theoretical analysis on capacity configuration for microgrid based on multi-agent system. *Electr. Power Energy Syst.* **2021**, *125*, 106485. [CrossRef]
14. Fang, F.; Zhongyan, Z.; Shunping, J.; Shiyan, H. Two-Layer Game Theoretic Microgrid Capacity Optimization Considering Uncertainty of Renewable Energy. *IEEE Syst. J.* **2021**, *15*, 4260–4271. [CrossRef]
15. Xue, M.; Zhao, B.; Zhang, X.; Jiang, Q. Integrated plan andevaluation of grid connected microgrid. *Autom. Electr. Power Syst.* **2015**, *39*, 6–13. [CrossRef]
16. Yuan, C.; Liu, G.; Wang, Z.; Chen, X.; Illindala, M.S. Economic power capacity design of distributed energy resources for reliable community microgrids. *Energy Procedia* **2017**, *142*, 2561–2567. [CrossRef]

17. Jing, Z.; Luo, Z. An IGDT model for capacity configuration optimization of island microgrid. *Energy Procedia* **2019**, *158*, 2774–2779. [CrossRef]
18. Zhang, X.; Shahidehpour, M.; Alabdulwahab, A.S.; Abusorrah, A. Security-constrained co-optimization planning of electricity and natural gas transportation infrastructures. *IEEE Trans. Power Syst.* **2015**, *30*, 2984–2993. [CrossRef]
19. Moradi, M.H.; Abedini, M. A novel method for optimal DG units capacity and location in microgrids. *Int. J. Electr. Power Energy Syst.* **2016**, *75*, 36–44. [CrossRef]
20. Zhang, H.; Xie, Z.; Lin, H.C.; Li, S. Power Capacity Optimization in a Photovoltaics-Based Microgrid Using the Improved Artificial Bee Colony Algorithm. *Applies Sci.* **2020**, *10*, 2990. [CrossRef]
21. Javadi, M.A.; Hoseinzadeh, S.; Ghasemiasl, R.; Heyns, P.S.; Chamkha, A.J. Sensitivity analysis of combined cycle parameters on exergy, economic, and environmental of a power plant. *J. Therm. Anal. Calorim.* **2019**, *139*, 519–525. [CrossRef]
22. Maraver, D.; Sin, A.; Sebastián, F.; Royo, J. Environmental assessment of CCHP (combined cooling heating and power) systems based on biomass combustion in comparison to conventional generation. *Energy* **2013**, *57*, 17–23. [CrossRef]
23. Xiao, H.; Pei, W.; Dong, Z.; Kong, L. Bi-level planning for integrated energy systems incorporating demand response and energy storage under uncertain environments using novel meta model. *CSEE J. Power Energy Syst.* **2018**, *4*, 155–167. [CrossRef]
24. Ju, L.; Tan, Q.; Lu, Y.; Tan, Z.; Zhang, Y.; Tan, Q. A CVaR-robust-based multi-objective optimization model and three-stage solution algorithm for a virtual power plant considering uncertainties and carbon emission allowances. *Int. J. Electr. Power Energy Syst.* **2019**, *107*, 628–643. [CrossRef]
25. Nosratabadi, S.M.; Hooshmand, R.A.; Gholipour, E. A comprehensive review on microgrid and virtual power plant concepts employed for distributed energy resources scheduling in power systems. *Renew. Sustain. Energy Rev.* **2017**, *67*, 341–363. [CrossRef]
26. Zhang, T.; Wang, M.; Wang, P.; Gu, J.; Zheng, W.; Dong, Y. Bi-stage stochastic model for optimal capacity and electric cooling ratio of CCHPs—A case study for a hotel. *Energy Build.* **2019**, *194*, 113–122. [CrossRef]
27. Sharafi, M.; ELMekkawy, T.Y. Multi-objective optimal design of hybrid renewable energy systems using PSO-simulation based approach. *Renew. Energy* **2014**, *68*, 67–79. [CrossRef]
28. Das, P.; Das, B.K.; Rahman, M.; Hassan, R. Evaluating the prospect of utilizing excess energy and creating employments from a hybrid energy system meeting electricity and freshwater demands using multi-objective evolutionary algorithms. *Energy* **2022**, *238*, 121860. [CrossRef]
29. Wang, X.; Chen, L.; Chen, Q.; Mei, Y.; Wang, H. Model and Analysis of Integrating Wind and PV Power in Remote and Core Areas with Small Hydropower and Pumped Hydropower Storage. *Energies* **2018**, *11*, 3459. [CrossRef]
30. Heide, D.; Von Bremen, L.; Greiner, M.; Hoffmann, C.; Speckmann, M.; Bofinger, S. Seasonal optimal mix of wind and solar power in a future, highly renewable Europe. *Renew. Energy* **2010**, *35*, 2483–2489. [CrossRef]
31. Sasikumar, C.; Manokar, A.M.; Vimala, M.; Winston, D.P.; Kabeel, A.E.; Sathyamurthy, R.; Chamkha, A.J. Experimental studies on passive inclined solar panel absorber solar still. *J. Therm. Anal. Calorim.* **2019**, *139*, 3649–3660. [CrossRef]
32. Manokar, A.M.; Vimala, M.; Sathyamurthy, R.; Kabeel, A.E.; Winston, D.P.; Chamkha, A.J. Enhancement of potable water production from an inclined photovoltaic panel absorber solar still by integrating with flat-plate collector. *Environ. Dev. Sustain.* **2020**, *22*, 4145–4167. [CrossRef]
33. Ming, B.; Liu, P.; Guo, S.; Zhang, X.; Feng, M.; Wang, X. Optimizing utility-scale photovoltaic power generation for integration into a hydropower reservoir by incorporating long- and short-term operational decisions. *Appl. Energy* **2017**, *204*, 432–445. [CrossRef]
34. Wang, S.; Jia, R.; Shi, X.; An, Y.; Huang, Q.; Guo, P.; Luo, C. Hybrid time-scale optimal scheduling considering multi-energy complementary characteristic. *IEEE Access* **2021**, *9*, 94087–94098. [CrossRef]
35. Hossain, M.A.; Pota, H.R.; Squartini, S.; Zaman, F.; Guerrero, J.M. Energy scheduling of community microgrid with battery cost using particle swarm optimisation. *Appl. Energy* **2019**, *254*, 113723. [CrossRef]
36. Anand, H.; Ramasubbu, R. A real time pricing strategy for remote micro-grid with economic emission dispatch and stochastic renewable energy sources. *Renew. Energy* **2018**, *127*, 779–789. [CrossRef]
37. Wen, X.; Xu, Z. Wind turbine fault diagnosis based on ReliefF-PCA and DNN. *Expert Syst. Appl.* **2021**, *178*, 115016. [CrossRef]
38. Fang, W.; Huang, Q.; Huang, S.; Yang, J.; Meng, E.; Li, Y. Optimal sizing of utility-scale photovoltaic power generation complementarily operating with hydropower: A case study of the world's largest hydro-photovoltaic plant. *Energy Convers. Manag.* **2017**, *136*, 161–172. [CrossRef]
39. Du, C.; Wang, X.; Wang, X.; Shao, C. A Block-Based Medium-Long Term Energy Transaction Method. *IEEE Trans. Power Syst.* **2016**, *31*, 4155–4156. [CrossRef]